

Near-Source Ground Motion along Strike-Slip Faults: Insights into Magnitude Saturation of PGV and PGA

by Jan Schmedes and Ralph J. Archuleta

Abstract Empirical data suggest that peak ground acceleration (PGA) and peak ground velocity (PGV) saturate as a function of magnitude for large magnitude ruptures close to the fault. Because data are sparse in the near-source region of large magnitude events, we have explored this question by simulating large magnitude strike-slip earthquakes. We use kinematic simulations to generate ground motion for a strike-slip fault that has a large aspect ratio (length/width). We consider both homogeneous or heterogeneous rupture models. We find that close to the fault along strike profiles of PGV and PGA increase to a maximum at a certain epicentral distance and then decrease to an asymptotic level beyond this distance. Critical factors for predicting ground motion are the position of an observer along strike, the depth of the hypocenter below the top of the fault, and the ratio of rupture velocity to shear-wave velocity. To understand the cause of the amplitude variation of along strike profiles of PGV and PGA, we use the isochrone method and the concept of the critical point to investigate how the geometry and kinematic parameters interact to produce the computed ground motion. We construct a predictor based on the critical point that does well in predicting the position of the maximum of PGV and PGA for stations close to the fault. For heterogeneous rupture models we find that the behavior is more complex though the general observation that along strike profiles of PGV and PGA increase to a maximum and then decrease still holds. This has implications for empirical attenuation relationships that essentially average the ground motion for all stations along strike with the same distance to the fault.

Introduction

One of the most important questions in seismic hazard assessment is how ground motion measures such as peak ground velocity (PGV) and peak ground acceleration (PGA) scale with magnitude. Recent empirical studies (Cua, 2004; Abrahamson and Silva, 2008; Boore and Atkinson, 2008; Campbell and Bozorgnia, 2008; Chiou and Youngs, 2008) find that PGA saturates with increasing magnitude, as stations get closer to the fault, whereas PGA increases with magnitude for stations farther away from the fault. That is, there is a distance dependent saturation of PGA with magnitude $\partial a/\partial M = f(r)$ (Rogers and Perkins, 1996). This is illustrated in Figure 1 (Boore and Atkinson, 2008). That is, for a fixed station with a small rupture distance (for example, 1 km), the PGA from an event with M_w 7 and from another event with M_w 7.5 will be the same; however, for a fixed station farther away (for example, 10 km), the PGA will be different for those two events (not shown in Fig. 1). In the following we will refer to this as distance dependent magnitude saturation. In this study we focus on the saturation of PGA and PGV (PGV does not fully saturate but does show a

decreased magnitude scaling close to the fault) with magnitude as shown in Figure 1.

There are many possible reasons for the observation of saturation of peak ground motion with magnitude. It could be caused by the dynamics of the earthquake rupture itself or by the geometry, for example, the aspect ratio, of large events, or it could be a sampling problem that results from having only a few near-source observations for large magnitude events. One approach for resolving this question is to use numerical simulations of earthquake ruptures. Rogers and Perkins (1996) used a finite fault statistical model to confirm the observed magnitude scaling. In their model the scaling arises from two principal sources: (1) isochrones that get longer for larger magnitudes yielding larger peak values and (2) extreme value properties because the number of patches with which the fault is constructed increases for larger magnitudes. Both effects yield larger ground motions for larger magnitudes at a given distance that is not too close to the fault. Close to the fault saturation occurs with magnitude because “only the closer portions of the fault dominate, almost

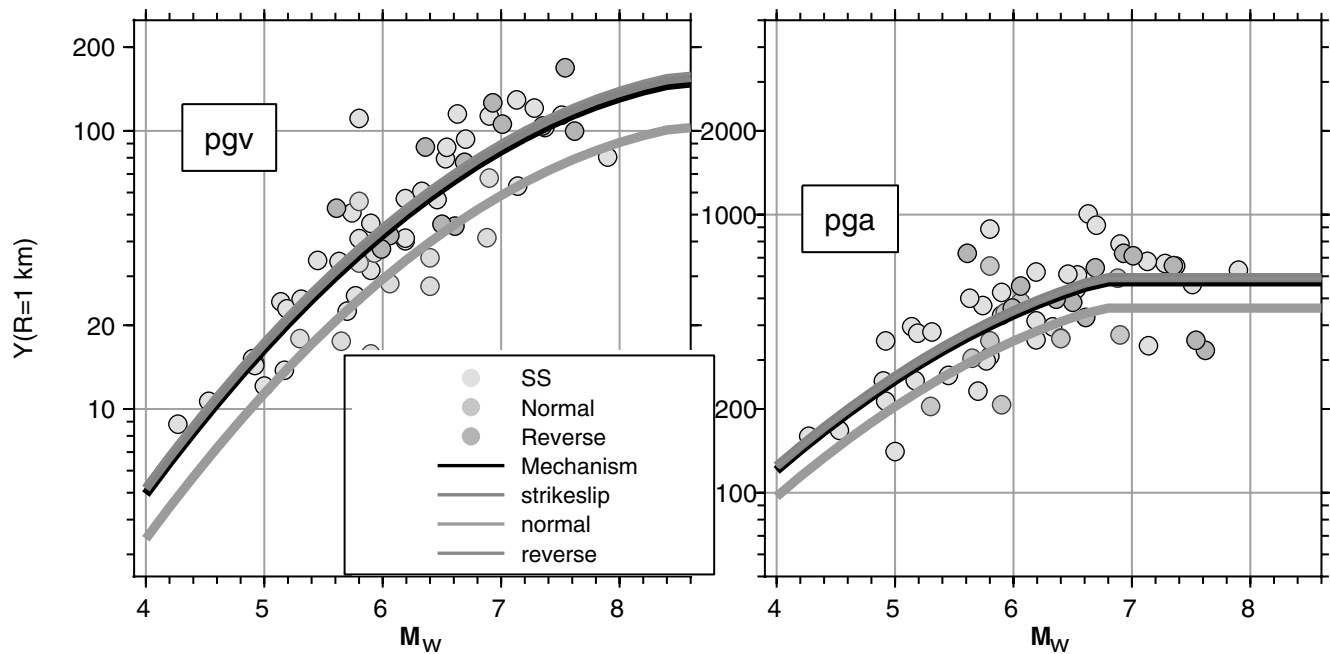


Figure 1. Example of magnitude saturation (modified from Boore and Atkinson [2008]). For distances close to the fault, the PGA at a given distance (for example, 1 km) is the same for all magnitudes with $M_w > 7$.

regardless of total rupture length” (Rogers and Perkins, 1996). Anderson (2000) also finds distance dependent magnitude saturation using different modeling techniques (combinations of empirical or theoretical Green’s functions and a simple or composite source representation). He concludes that the dependence of magnitude scaling with distance is a result of the Green’s functions that are more complex and have a longer duration for larger distances from the fault.

In this study we compute ground motion for long strike-slip earthquakes using a kinematic source model (Liu, *et al.*, 2006). We use isochrones (Bernard and Madariaga, 1984; Spudich and Frazer, 1984) to analyze the computed ground motion. Isochrones are the locus of points on the fault that radiate elastic waves all of which arrive at a given station at the same time. Each station has a different isochrone distribution; that is, each station sees different parts of the fault at a given time. Hence, isochrones can be used to extract that part of the rupture that produces a peak in the ground motion for a given station.

We analyze ground motions computed for homogeneous and heterogeneous earthquake sources using isochrones and discuss the implications that the distribution of ground motion has on empirical attenuation laws.

Geometry and Homogeneous Kinematic Model

First, we construct a simple kinematic source model for a strike-slip event with M_w 7.4 having constant slip, rise time, and subshear rupture velocity $v_{\text{rup}} = C\beta$, where $C = 0.8$ and β is the shear-wave velocity on a fault in a homogeneous elastic half-space. We use the slip rate function by Liu *et al.* (2006) with a rise time of 1.85 sec. It allows slip

at only one time and has a smoother shape than formulations using triangles that yield more high-frequency radiation. The Green’s functions are computed up to 10 Hz using the frequency-wavenumber ($f-k$) method (Zhu and Rivera, 2002). The vertical fault plane extends from 0.1 km below the surface to a depth of 15 km. The fault length is 115.5 km. The hypocenter is at a depth of 10.1 km. The elastic half-space has shear-wave velocity $\beta = 2.7$ km/sec, P -wave velocity $\alpha = 4.7$ km/sec, and density $\rho = 2500$ kg/m³. Rows of stations are distributed at the free surface parallel to the fault where X_S denotes the along strike distance from the epicenter (spacing between stations is 2.5 km) and at various distances measured perpendicular to the strike, $y = 2.5, 5, 10, 15, 20,$ and 25 km (Fig. 2).

Isochrone Theory and the Critical Point

For a given station and a single point on the fault, an arrival time (or isochrone time) is the sum of the time it takes the rupture front to reach a point on the fault plus the travel time from that point to the receiver. Isochrones (Bernard and Madariaga, 1984; Spudich and Frazer, 1984) are, thus, lines on the fault that connect the locus of points on the fault all of which have the same arrival time. The concept is illustrated in Figure 3 for two stations. Because each station has a different isochrone distribution, each observer on the surface sees different parts of the rupture at different times. For a given station, the area between two isochrones contours, corresponding to a time t and $t + \delta t$, radiates elastic waves that arrive at the corresponding station within the time increment δt . In Figure 3, note that, as the rupture approaches the station, the isochrones between the hypocenter and the station

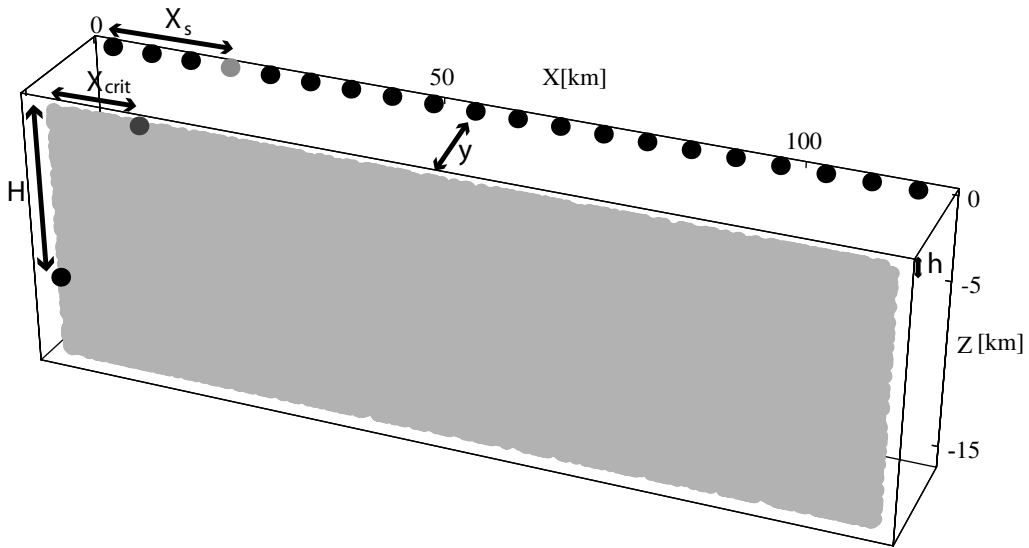


Figure 2. Geometry used in kinematic calculation. The vertical fault is the gray area. The black dot on the fault marks the hypocenter. As an example, if the lighter station is chosen, the dark gray point on the top of fault is the critical point (schematically) for that station (see text for explanation of critical point). H is the distance from the top of the fault to the hypocenter; h is the distance from the free surface to the top of the fault; y is the perpendicular distance from the strike to a line of stations parallel to the fault strike; and X_s is the distance measured from the epicenter along strike.

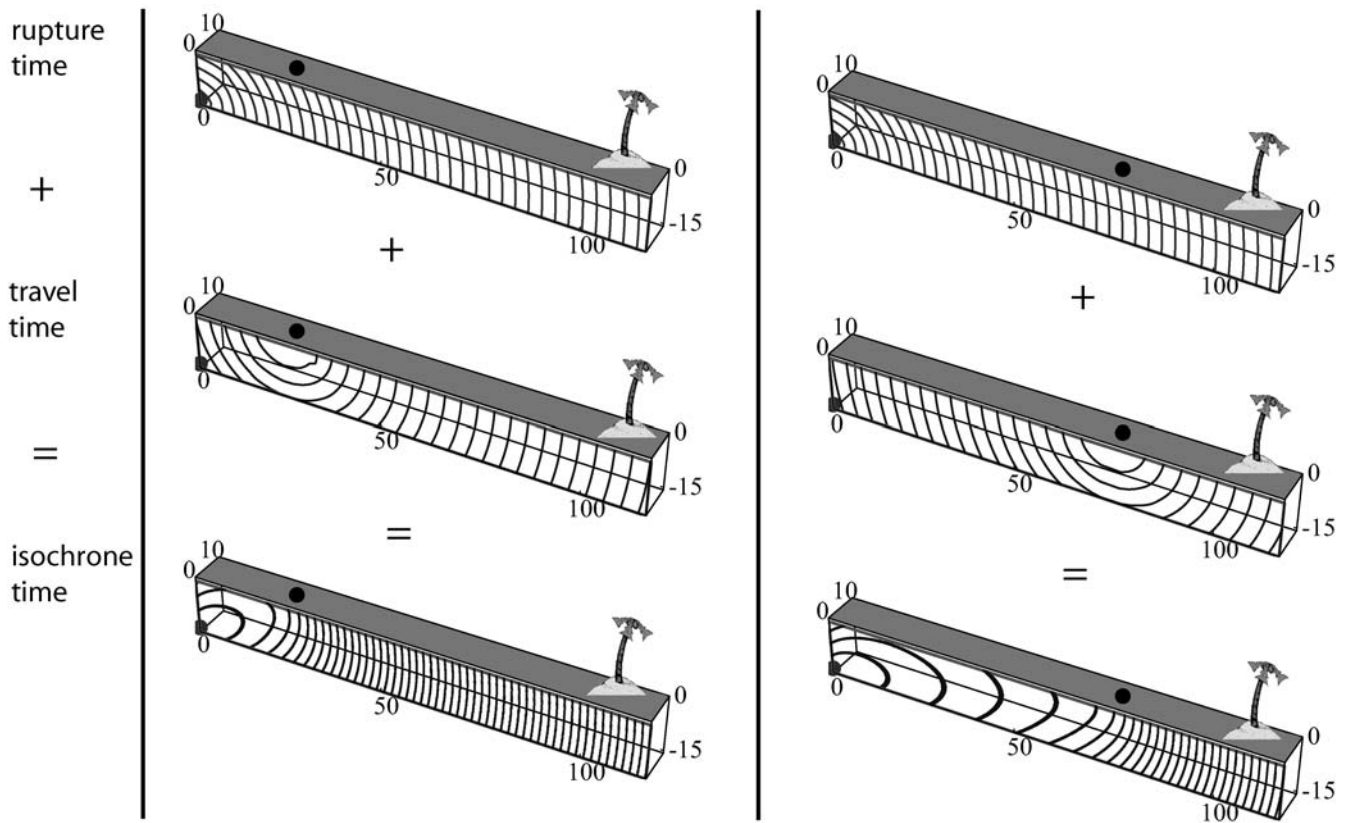


Figure 3. Top to bottom: Rupture time, travel time, and isochrone distribution for two different stations (black dots). While the rupture time distribution is the same for both, the travel times and hence the isochrone distributions are different. Isochrones are the locus of points that radiate elastic waves (P or S waves) that arrive at the station at the time corresponding to the time of the isochrone contour.

are widely spaced, encompassing large areas of the fault; whereas once the rupture front has passed the station, the isochrones are very closely spaced with a corresponding decrease in the area swept out in each δt . As the rupture front moves toward the station, the widely spaced isochrones are collecting radiation from large areas of the fault, and all this radiation is arriving in a short amount of time leading to large amplitudes, that is, directivity. Furthermore, between the hypocenter and the station there is strong deceleration and acceleration of the isochrones that will also produce strong radiation (see equation 1 and the following explanation).

According to isochrone theory, a strong phase is radiated from the isochrone that is tangent to a barrier because the isochrone gets discontinuous at this point (Bernard and Madariaga, 1984). To give more insight into why that is, we plot the isochrone contribution (following explanation) for a homogeneous rupture model as a function of time together with the ground acceleration (Fig. 4) computed using the

simple kinematic model for an M_w 7.4 strike-slip event described previously. To compute the isochrone contribution, we divide the fault into many subfaults and calculate the isochrone time for each subfault. Then we count the number of subfaults that fall into a time increment of 0.1 sec and multiply the number of subfaults by the area of each subfault. Hence, the isochrone contribution can be understood as the area that radiates elastic waves (in this example, S waves) that arrive at the station in a given time increment. First, the area is increasing as the isochrone's length, and velocity grows as the rupture propagates toward the station, that is, directivity. But once the isochrone becomes tangent to the top of the fault, future isochrones are discontinuous and do not add area in the upward direction resulting in a sharp decrease in the isochrone contribution (or a change of area). This abrupt change in the isochrone contribution when the isochrones get discontinuous is associated with a peak in the recorded ground velocity/acceleration. We will call the point

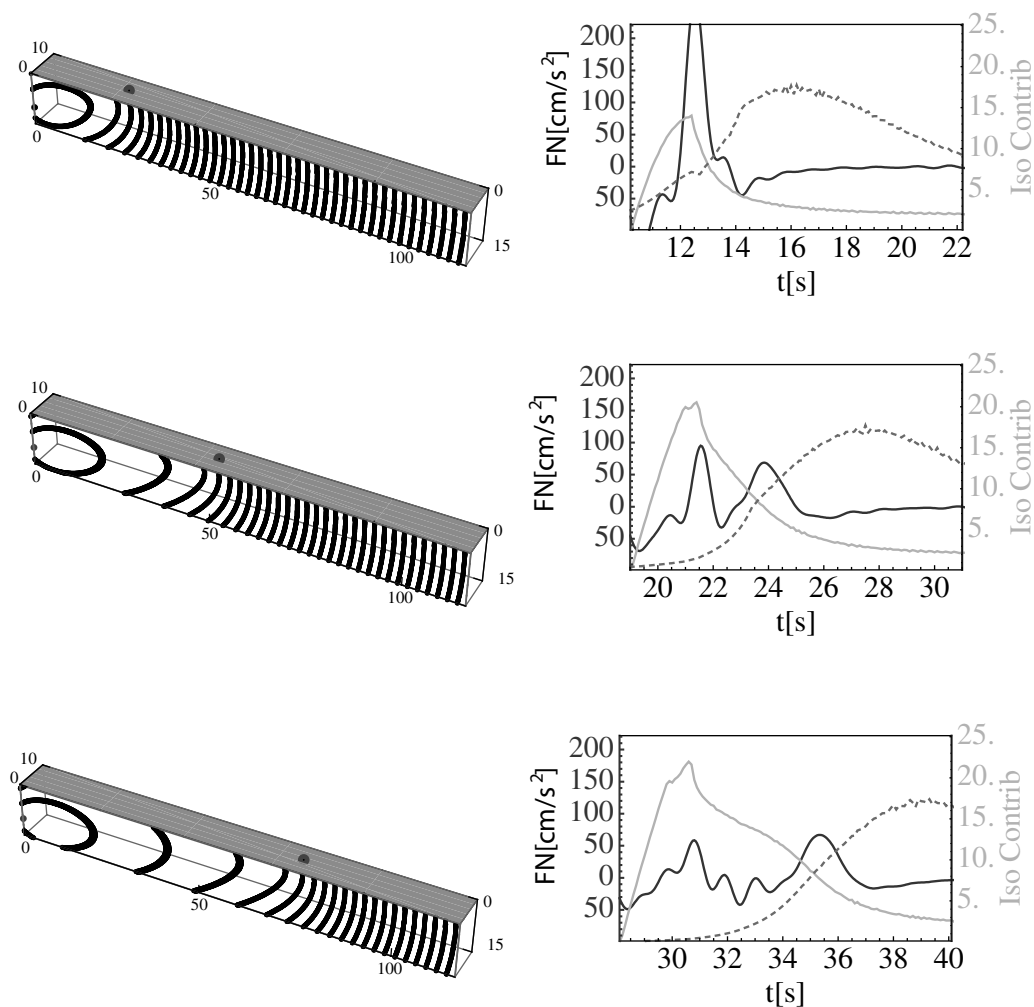


Figure 4. Left: Isochrone distribution for three different stations ($y = 5$ km) along strike. Right: We show (1) computed ground acceleration (FN component) in black, (2) computed isochrone contribution (area between two isochrone contours that are 0.1 sec apart) in gray, and (3) $1/R$, R being the mean distance to the isochrone, as dashed curves. No scale is given for $1/R$; it is plotted to get an idea of the relative amplitude of this term at different times. The peak occurs when the isochrone passes the station because this is the closest isochrone. Note that the FN component has a node in the radiation pattern for the closest isochrone.

at which the isochrone is first tangent to the top of the fault the critical point following Bernard and Madariaga (1984); this point can be associated with a peak in the computed ground acceleration. This peak can be identified for all three stations. However, because this peak is radiated from an earlier part of the rupture, geometrical spreading, that is, $1/R$, where R is the distance from each point on the isochrone to the station, attenuates this peak for more distant stations.

The representation theorem (equation 1), as written by Spudich and Frazer (1984) and modified by Zeng (1991), clearly shows why ground acceleration for a homogeneous rupture is proportional to the change in isochrone contribution:

$$\hat{\mathbf{a}}\ddot{u}^p(\mathbf{x}, t) = -\ddot{f}_r(t)^* \int_{y(t,\mathbf{x})} \left[\frac{ds_r}{dq} \mathbf{G}_a^p c^2 + s_r \frac{d\mathbf{G}_a^p}{dq} c^2 + s_r \mathbf{G}_a^p \frac{dc}{dt} + \kappa s_r \mathbf{G}_a^p c^2 \right] dl. \quad (1)$$

In equation (1) the component of ground acceleration in the direction $\hat{\mathbf{a}}$ resulting from wave type p is the convolution of the time derivative of the slip velocity time function \dot{f} and the integral along the isochrone over the sum of four terms: (1) the product of spatial change of slip s on the fault and the k component of the Green's function G , scaled by the squared isochrone velocity; (2) the spatial change of the Green's function times the slip on the fault, scaled by the squared isochrone velocity; (3) the slip on the fault times the Green's function, scaled by the temporal change of the isochrone velocity; and (4) a term that is the product of the curvature κ of the isochrone, the squared isochrone velocity, the Green's function, and the slip. The isochrone velocity can be computed as the inverse of the norm of the spatial gradient of the isochrone time (Spudich and Frazier, 1984). Therefore, the widely spaced isochrones that run toward the station (Fig. 3) correspond to a large isochrone velocity. Note, that even though the rupture velocity is constant, the isochrone velocity is not.

Hence, besides spatial variations in slip and spatial variations in the Green's functions on the fault (this can often be neglected), a large isochrone velocity itself and/or large changes in isochrone velocity can produce large ground motion. An additional contribution comes from the last term involving the curvature. For two isochrone segments of the same length, this term will be larger for the isochrone with the larger curvature.

In the case of a homogeneous rupture (constant slip), the first integrand can be set to zero. In the case of a homogeneous half-space and continuous isochrones, the second integrand will be small because the Green's functions do not change significantly along the isochrones. Thus, ground acceleration in this simple case is mainly proportional to changes in the isochrone velocity and to places on the fault that have long isochrones with large curvature.

Because the largest change in the isochrone contribution occurs when the rupture hits the top of the fault (in this model) where the isochrone becomes discontinuous, the critical point produces the greatest radiation. Note that the isochrone that first becomes tangent to the top of the fault is also the longest (in this homogeneous case) and it has a larger curvature than isochrones at a later time also yielding a strong contribution from the last term in equation (1). Because the critical point is the first of all points at the top of the fault that is reached by the isochrones, it has the minimal isochrone time for all these points. This time can be determined using equation (2):

$$T_{\text{iso}} = \sqrt{(X_s - X_{\text{top}})^2 + y^2 + h^2} / \beta + \sqrt{X_{\text{top}}^2 + H^2} / v_{\text{rup}}, \quad (2)$$

where X_{top} is the along strike coordinate of the points at the top edge of the fault; y , h , H , and X_s are defined in Figure 2; and v_{rup} and β are the rupture velocity and shear-wave velocity, respectively.

Because the critical point has the minimum isochrone time, it is possible to compute the position X_c of the critical point for a given station by setting the partial derivative of equation (2) with respect to X_{top} to zero. Thus, for every point on the free surface we can compute the point on the top of fault that produces the strongest radiation. Another critical point is at the end of the rupture, that is, the stopping phase. By equating the isochrone time for the end of the fault and solving for the minimal isochrone time, one can compute that critical point as well.

Computed PGV and Explanation Using the Critical Point

In Figure 5 we plot the computed PGV for fault parallel (FP) and fault normal (FN) and the position X_c of the critical point as a function of the along strike distance X_s for different values of y . The along strike profile of PGV shows an increase until a maximum value and then a decrease, especially on the FN component. This decline of PGA with distance along strike for a long strike-slip rupture was also observed in other studies (Spudich and Chiou, 2008) but has not been explained yet. The position of the peak, moving along strike, depends on y and on the value of H and C (see the section Influence of H and C). The shape of the peak amplitude along strike can be understood by considering the position of the critical point. As X_s increases for a station, the critical point also moves away from the epicenter. After a while even though X_s continues to increase, the critical point stays at approximately the same place. Geometrical spreading ($1/R$) attenuates the ground motion resulting from the critical isochrone. Hence, the maximum ground velocity for stations with large X_s is produced by an isochrone close to the station. However, the isochrone contribution that is close to the station has weaker radiation (isochrones are more

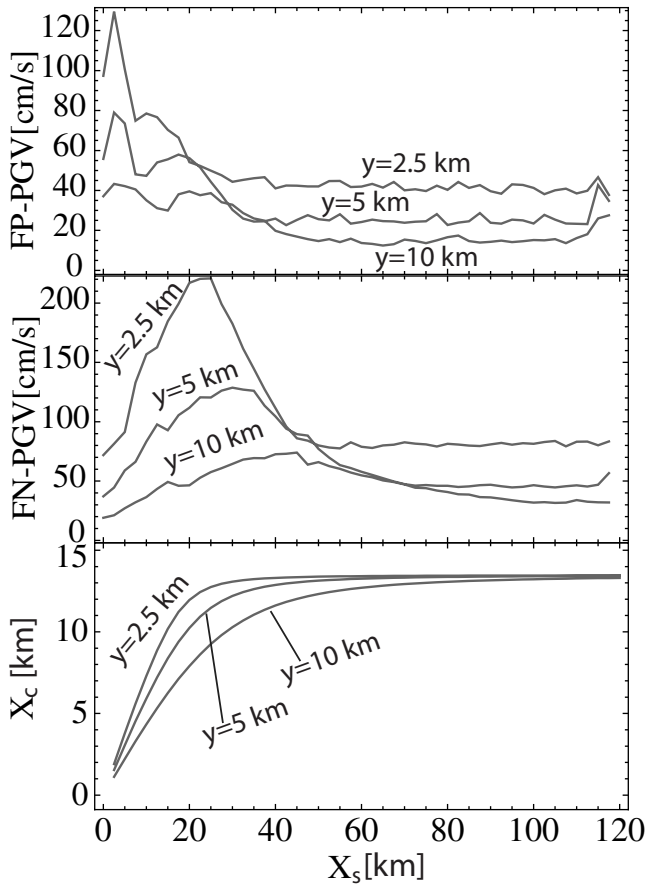


Figure 5. Top: FP PGV as a function of distance along strike for different y , a distance measured perpendicular to the fault strike. The three curves in each plot are computed using homogeneous rupture models with different values of y . Middle: FN PGV. Bottom: Along strike position of the critical point plotted as a function of the along strike position of the station. For stations close to the fault ($y = 2.5$ and 5 km), the critical point stays approximately at the same position for distances farther along strike. With $1/R$ attenuating the radiation from the critical point, the PGV of the stations far from the critical point comes from an isochrone close to the station. This isochrone has weaker radiation than that from the critical point.

closely spaced, shorter, and with less curvature); thus, the PGV is smaller than for stations close to the critical point. This is the basic reason for the shape of along strike profiles of PGV (and PGA). As y increases, that is, the line of stations parallel to the fault moves farther from the fault, the peak in PGV occurs at a larger X_s distance.

The critical point affects the FN component more than the FP component because the radiation becomes strongest for stations a certain distance away from the critical point due to the stronger directivity effect (see also the next section). The FN component is sensitive to the history of the rupture, that is, what happens before the isochrones come close to the station. For this reason the directivity is observed primarily on the FN component. The FP component is more sensitive to what happens near the station. Because the isochrone velocity and changes in the isochrone velocity are largest at the

beginning of the rupture, the FP component has its maximum in the epicentral region. In the case of a heterogeneous rupture, asperities and strong local changes in the isochrone velocity can produce strong radiation in regions distant from the epicentral region (see the later section on heterogeneous ruptures).

Predictor of the Shape of the PGV and PGA Curves

For stations at a fixed y , the distribution of PGV along strike is caused by the critical point. Knowing the position of the critical point, one can compute the effect of geometrical attenuation $1/R$. But in order to predict where the strongest ground motion will occur at a given distance from the fault, one needs to know how strongly the critical point radiates. In our homogeneous model the radiation is proportional to the change in the isochrone contribution. Within a given time increment the more points at the top edge of the fault that radiate, the larger is the change in the area because no more rupture area is added in the upward direction. In Figure 6 we plot the isochrone time for the points at the top edge of the fault according to equation (2) for two stations. For the station with a greater X_s distance, a longer segment of the top edge of the fault radiates elastic waves that arrive at the station within 0.5 sec after the critical phase. The reason is that the curve describing the isochrone time as a function of position along the top of the fault has a smaller curvature for the more distant station. The change in isochrone contribution is hence inversely proportional to the curvature of this curve evaluated at the critical point (equation 1). Thus, we construct a predictor for the relative amplitudes in ground motion due to radiation from the critical point. To account for the radiation we evaluate the curvature, that is, the inverse of the second derivative of equation (2), at the critical point and multiply it by the inverse distance (geometrical spreading) to the critical point. This yields

$$\text{predictor}(y, h, H, X_s, \beta, C) = [T''_{\text{iso}}(X_c) \sqrt{X_c^2 + y^2 + h^2}]^{-1}. \quad (3)$$

This predictor cannot be used to predict absolute amplitudes, but it can predict the shape of the curve around the maximum of the PGV and PGA. A comparison of the predictor and the PGV and PGA (here for ground motion up to 1 Hz) along strike profiles plots for different y is given in Figure 7. In all cases the position of the maximum on the FN component is predicted well, especially close to the fault. Because the predictor predicts only the shape that results from the critical point, the tail of the curves produced by radiation close to the recording stations is not predicted. Note, that the general behavior of PGA is similar to PGV: there is a similar shape of the along strike profiles very close to the fault. For increasing y the PGA and PGV saturate for lines of stations parallel to the fault strike. For even larger y , the PGA and

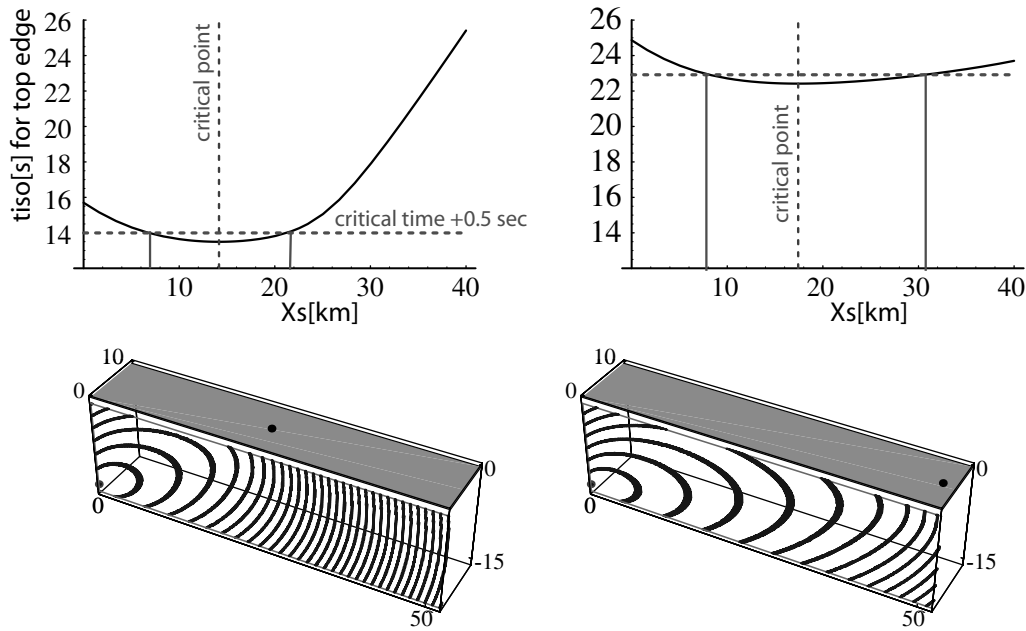


Figure 6. Top: Isochrone time of the top edge of the fault for two stations. The minimum corresponds to the critical point. The curvature of the curve defines how much isochrone contribution will be missing for a given time increment because the isochrone cannot extend above the top edge of the fault. Hence, a small curvature yields a strong change in the isochrone contribution. Bottom: Isochrones for the two stations (black dots at about 20 and 50 km) are plotted for the first 50 km of the fault.

PGV will increase along strike—with no evidence of saturation.

Implications of the Spatial Dependence of PGV and PGA for Empirical Studies

Most attenuation relations use either the closest distance to the fault or the distance to the surface projection of the fault as the distance measure (Abrahamson and Shedlock, 1997). In our idealized model, both of these distance measures would group all stations that have the same value of y . In an earthquake, there might be only one or two stations

close to the fault strike. Given the form of PGV and PGA plotted along strike of the fault, the small number of stations can produce a sampling issue. If a station were at the end of the rupture, the recorded PGV in our model at $y = 5$ km would be 40% smaller than if the station were in the area around the maximum PGV. Moreover, the longer the fault rupture length, the more likely the station will be in an area where the ground motion is reduced relative to the maximum. However, for a smaller rupture length a station close to the fault rupture is more likely to sample the area where the maximum PGV and PGA occur. Thus, if there is only one station close to the fault that ruptures, this station will likely

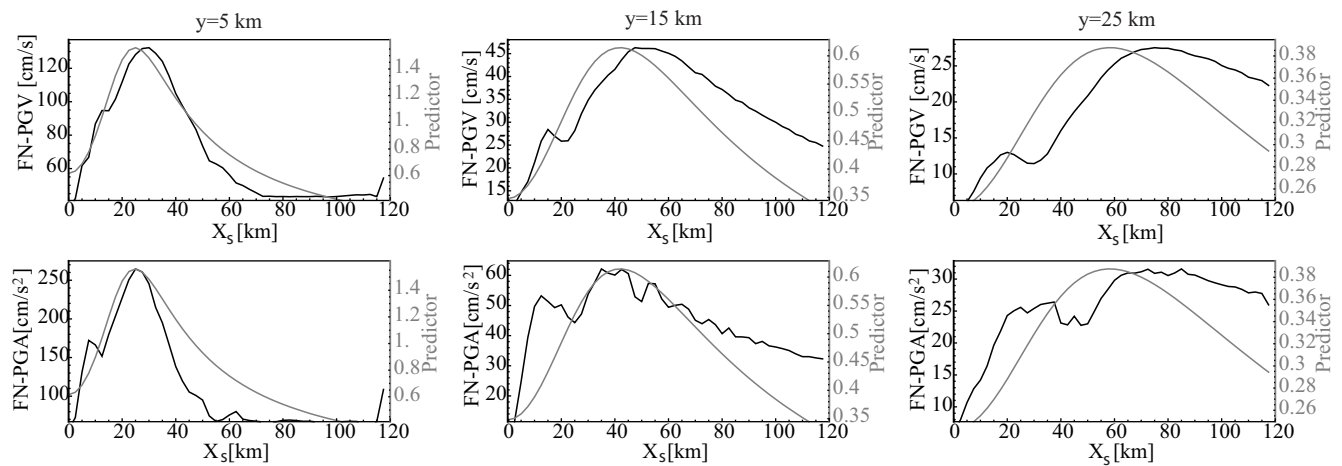


Figure 7. Computed PGV and PGA along strike (black curves, scale at the left) for different distances (y) to the fault. The predictor (gray curves, scale at right) is computed using equation (3). Note that the peaks of the predictor and the peaks of the PGV/PGA generally agree, especially for stations close to the fault ($y = 5$ km). Furthermore, the amplitudes agree, that is, a larger predictor corresponds to a larger PGV.

record about the same PGV or PGA for two different magnitudes simply because the stations sample different parts of the rupture for the two events.

Consider what we observe in an ideal world where stations are distributed equally along the fault. Let us further assume that there is constant stress drop and that all events rupture the full width of the fault. Then the magnitude of the earthquake scales only with the rupture length because the average slip is also constant. This assumption is only valid for earthquakes with a magnitude greater than some minimum because smaller magnitude events would not rupture the full width of 15 km. In Figure 8 we plot the along strike profiles for $y = 5$ km for $M_w 7.4$ and $M_w 7.3$ ruptures. Both earthquakes have the same slip, rise time, and rupture velocity; only the rupture length is different (80 km for the $M_w 7.3$ rupture). For the stations that lie next to both ruptures, that is, within 0–80 km, the two (solid) curves are almost identical. The seismograms of both events have different durations, but the peak values are identical. In a regression relation the solid parts of the profiles (Fig. 8) would be averaged for both events because those stations are 5 km from the projection of the rupture plane. The average value for the $M_w 7.3$ rupture in this example is close (it is actually slightly larger) to that of the $M_w 7.4$ rupture. That is, there is magnitude saturation of the peak values for distances close to the fault.

For larger y the maximum of the along strike profile is shifted away from the epicenter due to the greater distance of the critical point from the hypocenter. Thus, the portion of the along strike profile that is decreasing, after the maximum value is reached, gets shorter with increasing y (see Fig. 7). For large enough y , the along strike profiles for different magnitudes will show only monotonic increase, yielding an

increasing average PGV and PGA with magnitude for all stations with the same distance to the rupture plane.

This is consistent with the finding (Cua, 2004; Abrahamson and Silva, 2008; Boore and Atkinson, 2008; Campbell and Bozorgnia, 2008; Chiou and Youngs, 2008) that magnitude saturation is observed only close to the fault; whereas, there is still an increase in PGV and PGA away from the fault.

Influence of H and C

In Figure 9 we plot the PGV and PGA (both for ground motion low-pass filtered to 1 Hz) along the fault for $y = 5$ km for two different hypocenter depths, $H = 6$ km and $H = 10$ km, and for two different values for the ratio of rupture velocity to shear-wave velocity, $C = 0.8$ and $C = 0.9$. The maximum PGV for the scenario with smaller H appears at a smaller epicentral distance (for $C = 0.8$) because the critical point reaches its limiting position closer to the epicenter allowing for greater effect of geometrical spreading $1/R$. The second, smaller local maximum for $H = 6$ km is produced by the critical point at the bottom of the fault. This peak is smaller because the rupture front is propagating away from the station; consequently, the isochrone contribution from the bottom of the fault is smaller than from the top of the fault. If the distance between the hypocenter and the bottom of the fault is small, as in the case of $H = 10$ km, this second peak does not appear because the radiation is too weak. The distance of the hypocenter from the top of the fault might also play a role in understanding why surface ruptures appear to have lower ground motion than buried ruptures (Somerville, 2003; Kagawa, *et al.*, 2004).

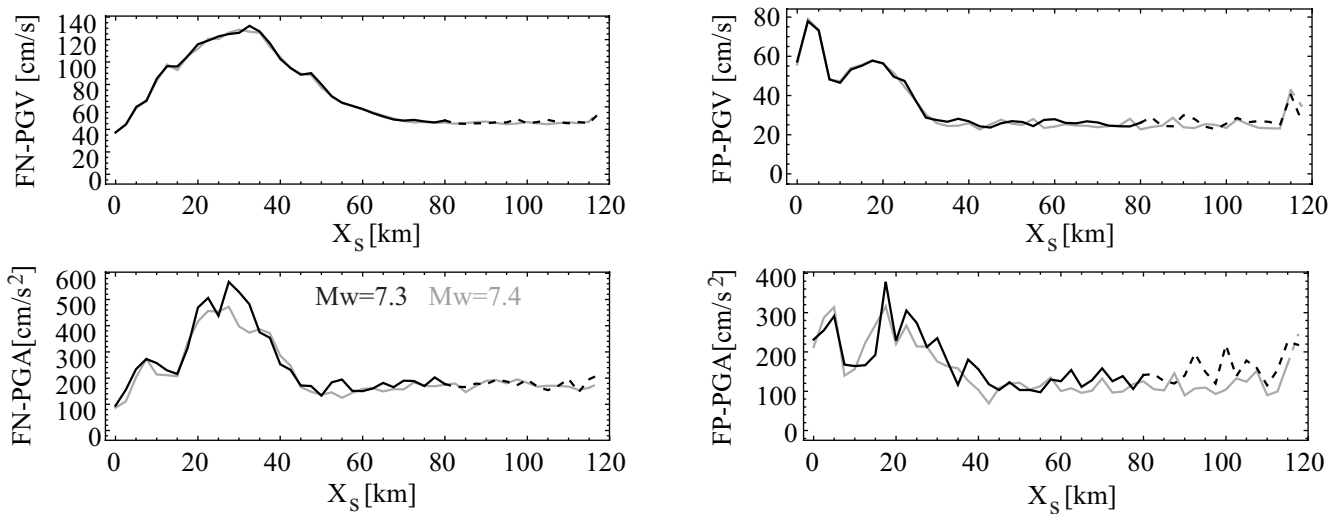


Figure 8. Computed PGV and PGA along strike for two events: $M_w 7.3$ (black) and $M_w 7.4$ (gray) and $y = 5$ km. The solid part of the black curve represents the stations that are 5 km from the projection of the fault to the surface. Because both models have identical slip, rise time, and rupture velocity, this initial part of the curve overlaps the gray curve because the isochrones on the first 80 km of the rupture are the same for both events. The stations corresponding to the dashed parts of the curve have an X_s that is greater than the rupture length for the given magnitude; thus, these stations have a closest distance to the projection of the fault plane to the surface that is larger than 5 km.

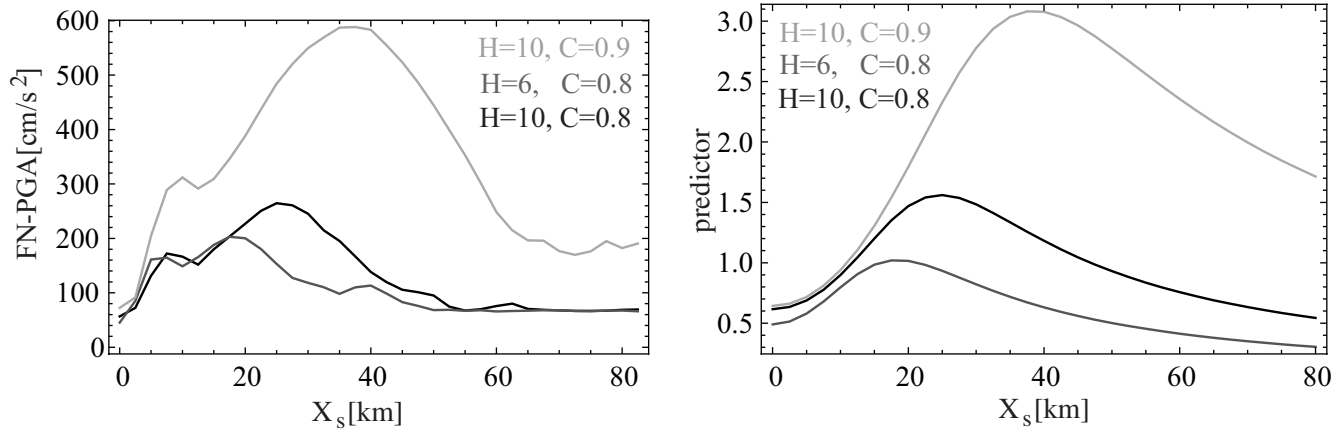


Figure 9. Left: PGA computed for different values of C (ratio of rupture velocity to shear-wave speed) and H (depth of the hypocenter). With $C = 0.8$ one can see that changing H results in a different position and amplitude of the maximum of the along strike profile. For the case with $H = 6$ km one can see a second small local maximum at about 40 km along strike after the main maximum. This small peak corresponds to the critical point at the bottom of the fault. By increasing C the overall PGA is increased significantly. In addition, the maximum PGA occurs at a distance farther from the epicenter. Right: The predicted shape of the PGA profile from the three scenarios using our predictor (equation 3). The position of the peaks as well as the relative amplitudes are predicted well.

Comparing the scenarios with $C = 0.8$ and $C = 0.9$, one can see a large difference in the amplitudes. The peak for $C = 0.9$ is farther along strike because the critical point reaches its final position farther along strike. The amplitudes are larger because the radiated waves arrive at the stations in a shorter time span due to the faster rupture velocity. This again illustrates the importance of the rupture velocity on ground motion.

In Figure 9 we have also plotted the predictor (equation 3) for comparison. It predicts the positions of the main peaks and the relative amplitudes well. It is, hence, a useful tool to get an idea of how different parameters affect the ground motion in the homogeneous model.

Slip Scaling

To study the effect of the observed PGV and PGA profiles on magnitude scaling for events with magnitude-dependent slip, we compute ground motion for events with different magnitudes. The top edge of all models is buried 100 m below the free surface. The length of the rupture is computed using the regression relations of Wells and Coppersmith (1994) for rupture area (for strike-slip faults) divided by a width of 15 km for all events. The constant slip is then computed to match the seismic moment. The rupture velocity is

set to 80% of the shear-wave velocity. Table 1 lists the values used in the computations. The hypocenter is always at $H = 10$ km.

Figure 10 shows the resulting along strike profiles for PGV and PGA and $y = 5$ km. For a given magnitude (and hence rupture length), the fraction of the profile that has a distance of 5 km to the projection of the rupture plane to the free surface is plotted as solid curves. These stations are right next to the rupture. The dashed parts of the curves correspond to stations that also have $y = 5$ km, but their closest distance to the rupture plane is farther away because their along strike distance X_s is larger than the rupture length for the given magnitude. That is, in terms of regression relations the solid parts of the curves should be compared. The solid parts of the curves do not overlay as in the previous section, but they have the same shape. While the amplitudes of the curves and the tails of the curves differ for PGV, they are similar for PGA. The average PGV and PGA for the different magnitudes are given in Table 1. While there is an increase for the PGV, the PGA for M_w 7.0, 7.2, and 7.4 are about the same for $y = 5$ km (similar to Fig. 1).

The shape of the along strike profiles differs for the dashed parts of the curve where the stopping phase can be observed. Note that for PGA the stopping phase produces even larger amplitudes than the critical point at the top of

Table 1

Values Used in Computation and Resulting Average PGV and PGA for Stations that Have a Distance to the Projection of the Fault to the Surface of 5 km

M_w	Length (km)	Slip (m)	Rise Time (sec)	PGV (cm/sec) at 5 km	PGA (cm/sec ²) at 5 km
6.6	22.08	1.48	1.07	30.6	143.4
6.8	33.41	1.96	1.34	45.0	184.3
7.0	50.58	2.57	1.43	57.9	216.1
7.2	76.54	3.39	1.78	63.2	193.5
7.4	115.85	4.46	1.85	70.1	218.8

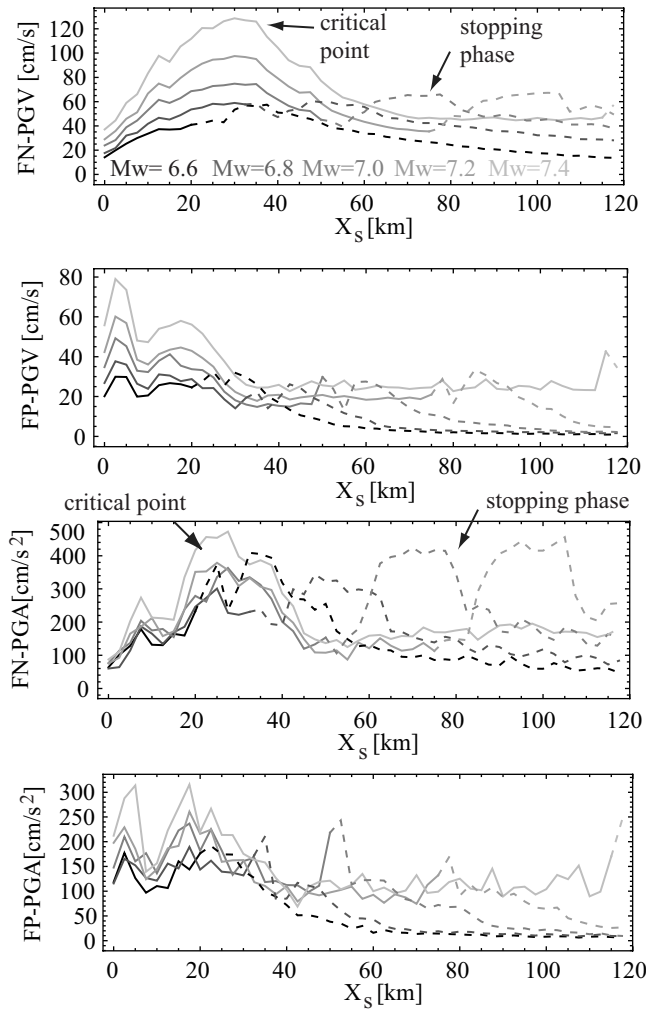


Figure 10. FN and FP PGV and PGA at $y = 5$ km for five events of different magnitude (see text). The kinematic source parameters are constant for all five events with only the slip being different to produce different magnitudes. The solid part of each curve represents the stations that are at a distance of 5 km to the projection of the fault plane to the free surface. The stations corresponding to the dashed parts of the curves have an X_s that extends beyond the rupture length for the given magnitude; thus, for these stations the closest distance to the projection of the fault plane to the surface is greater than 5 km. The solid parts of the PGA curves are very similar, even though the magnitudes of the events are different. The dashed parts of the curves show a second maximum, especially for PGA, which corresponds to the stopping phase. Note that this maximum from the stopping phase has the same or even larger amplitude than the maximum corresponding to the critical point at the top edge of the fault.

the fault. These large amplitudes appear at a distance larger than 5 km.

Heterogeneous Rupture Models in a Layered Velocity Model

So far we have performed computations for homogeneous rupture models in an elastic half-space. But does the overall behavior of PGV and PGA along the fault hold for

heterogeneous rupture models in a layered velocity structure? We use the method of Liu *et al.* (2006) to construct rupture models that have correlated kinematic parameters. There will be positive spatial correlation on the fault between slip and rupture velocity and between slip and rise time. Areas with large slip are likely to have a larger rupture velocity and longer rise time than areas with small slip. The slip is spatially coherent with a von Karman distribution for the wavenumber (Mai and Beroza, 2002); the amplitudes follow a truncated Cauchy distribution (Lavallée and Archuleta, 2003). The average rupture velocity of each subfault in the kinematic model takes values between $C = 0.6$ and 1 following a uniform distribution. Note that the rupture can locally go supershear (for example, Burridge, 1973; Andrews, 1976; Archuleta, 1984; Bouchon *et al.*, 2001; Bouchon and Vallée, 2003; Dunham and Archuleta, 2004) yielding very different behavior from a subshear rupture. We use a layered 1D velocity structure given in Table 2 to compute the Green's functions.

As might be expected, the computed PGV and PGA curves (Fig. 11) are more complex for the case of rupture in a layered medium. However, the general shape of the along strike profiles of PGV and PGA can still be observed. For heterogeneous models, especially with variable rupture velocity, we cannot use the concept of one critical point to explain the behavior of PGV along the fault. The ground motion in a completely heterogeneous model will depend not only on the changes in isochrone contribution but also on the isochrone contribution itself as well as variations in slip along the isochrones (equation 1) and changes in isochrone curvature. Hence, every area with large values of slip or rupture velocity, or with a sudden change in rupture velocity or slip on the fault, can produce strong radiation (Spudich and Frazer, 1984). This can be observed in Figure 11 for the longest rupture. On both components there are local maxima in PGV and PGA that are not due to the critical point but are due to local areas of large values or changes of values of slip and rupture velocity. The predictor with one critical point will not work anymore. To mimic different critical points one could take the average of a set of predictors computed by using random values of C .

The reason for the basic shape of the profile (at constant y) is again primarily geometrical spreading, which has a strong relative effect for stations that are close to the fault.

Table 2

1D Velocity Structure Used in the Computations with Heterogeneous Source Models

V_P (m/sec)	V_S (m/sec)	Density (kg/m^3)	Thickness (m)	Q_P	Q_S
3600	1800	2400	150	60	30
4100	2200	2500	450	120	60
4700	2700	2600	700	200	100
5400	3100	2700	1000	320	160
5900	3400	2800	1700	500	250
6300	3600	2900	23000	1000	500
7800	4500	3300	—	1000	500

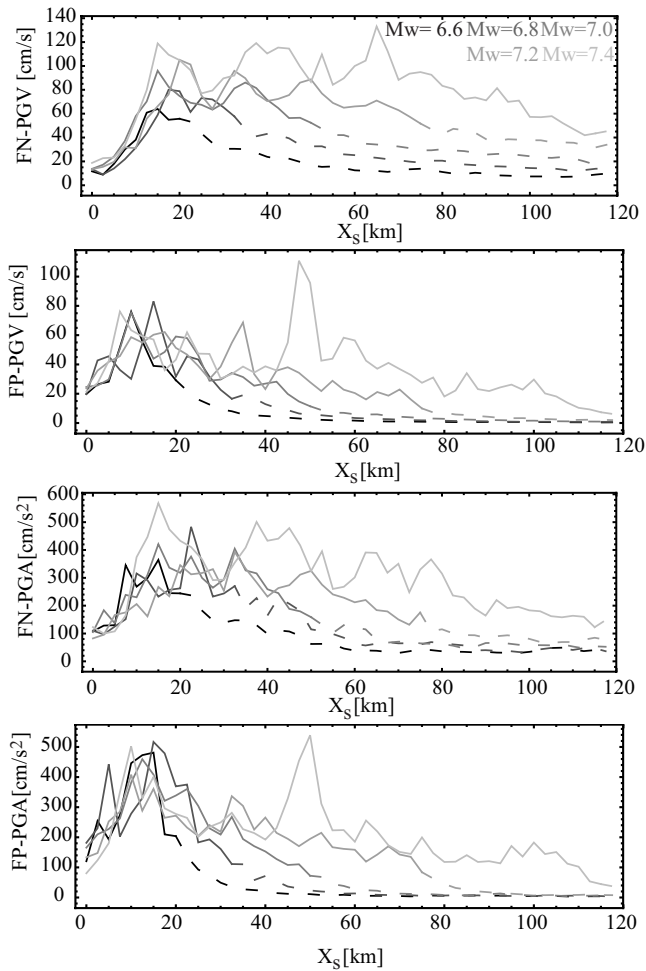


Figure 11. FN and FP PGV and PGA for five events with different magnitudes. All profiles are for a distance $y = 5$ km. A heterogeneous kinematic source model based on the method of Liu *et al.* (2006) was used to compute the ground motion. A layered 1D velocity structure (Table 2) was used. The solid part of each curve represents the stations that are at a distance of 5 km to the projection of the fault plane to the free surface. The stations corresponding to the dashed parts of the curve have an X_s that extends beyond the end of the rupture for the given magnitude; thus, for these stations the closest distance to the projection of the fault plane to the surface is greater than 5 km. The solid parts of the PGA curves are very similar, even though the magnitudes of the events are different. In general, more than one maximum can be observed due to either large slip patches or abrupt changes in rupture velocity. But the overall shape also shows an increase in the beginning of the rupture plane and a decrease at the end of the rupture plane. Note that the stopping phase cannot be observed in the dashed parts of the curves as in Figure 10.

At the beginning of the rupture, the isochrone velocity is the largest. Hence, a change in slip in the early part of the rupture radiates more strongly than the same change would in a later part of the rupture (first integrand in equation 1). Furthermore, there are larger changes in the isochrone contribution in the first part of the rupture due to directivity, and the curvature and length of the isochrones is larger in the earlier part of the rupture. Thus, a patch with large slip will radiate more strongly at the beginning of the rupture than at the end. That

is, a station close to a large slip patch at the beginning of the rupture will experience stronger peak ground motion than a station close to a large slip patch at the end of the rupture. Even though the rupture is heterogeneous, there will still be a change in isochrone contribution associated with the isochrone hitting the top of the fault, which will also happen in the earlier part of the rupture. Because $1/R$ attenuates the radiation from the earlier part of the rupture for stations farther along strike, we expect lower ground motion from the earlier part of the rupture for stations farther along strike from the epicenter.

Note that in Figure 11 the radiation from the stopping phase cannot be observed. This observation also holds for heterogeneous models in an elastic half-space that we performed. For the homogeneous models the isochrone that produces the stopping phase is close to a straight line and is coincident with the straight edge of the end of the fault. Thus, the isochrone abruptly stops producing a strong stopping phase (see Fig. 6). In terms of our predictor the isochrone time plotted as a function of the coordinate along the end of the fault has a very small curvature. For the heterogeneous model the end of the fault will not be coincident with a single isochrone, and thus it will produce less radiation. This effect depends on the degree of heterogeneity of the rupture velocity. Because our model has a very high heterogeneity in the rupture velocity, the stopping phase is not observed. For more smooth heterogeneous models we might expect to see a phase corresponding to an isochrone becoming tangent to the end of the fault plane.

To prevent any bias arising from the results of only one random model for each magnitude, we computed ground motion for six random kinematic source models for each magnitude. Out of all models and stations for a given closest distance to the projection of the fault plane to the surface, we selected randomly 50 PGA and PGV values for each magnitude. In Figure 12 the average PGV and PGA values are plotted with ± 1 standard deviation for $y = 5$ km and $y = 25$ km. For $y = 25$ km both PGV and PGA show scaling with magnitude, that is, they both increase with increasing magnitude. The PGV for $y = 5$ km does also increase with magnitude, but the relative increase of PGV for an event with $M_w 7.4$ with respect to an event with $M_w 6.6$ is larger for $y = 25$ km than for $y = 5$ km. The PGA at $y = 5$ km shows saturation; it even shows a smaller average for an $M_w 7.2$ event than for an $M_w 7.0$ event. We attribute this to the small number of PGA values for which this curve is created. But the general observation that PGA saturates with magnitude for stations close to the fault and increases with magnitude for stations farther away from the fault is reproduced by our simulations and explained in the previous paragraphs.

Conclusions

We computed ground motion from kinematic simulations of earthquakes on a long strike-slip fault using homogeneous and heterogeneous rupture models. In both cases, at

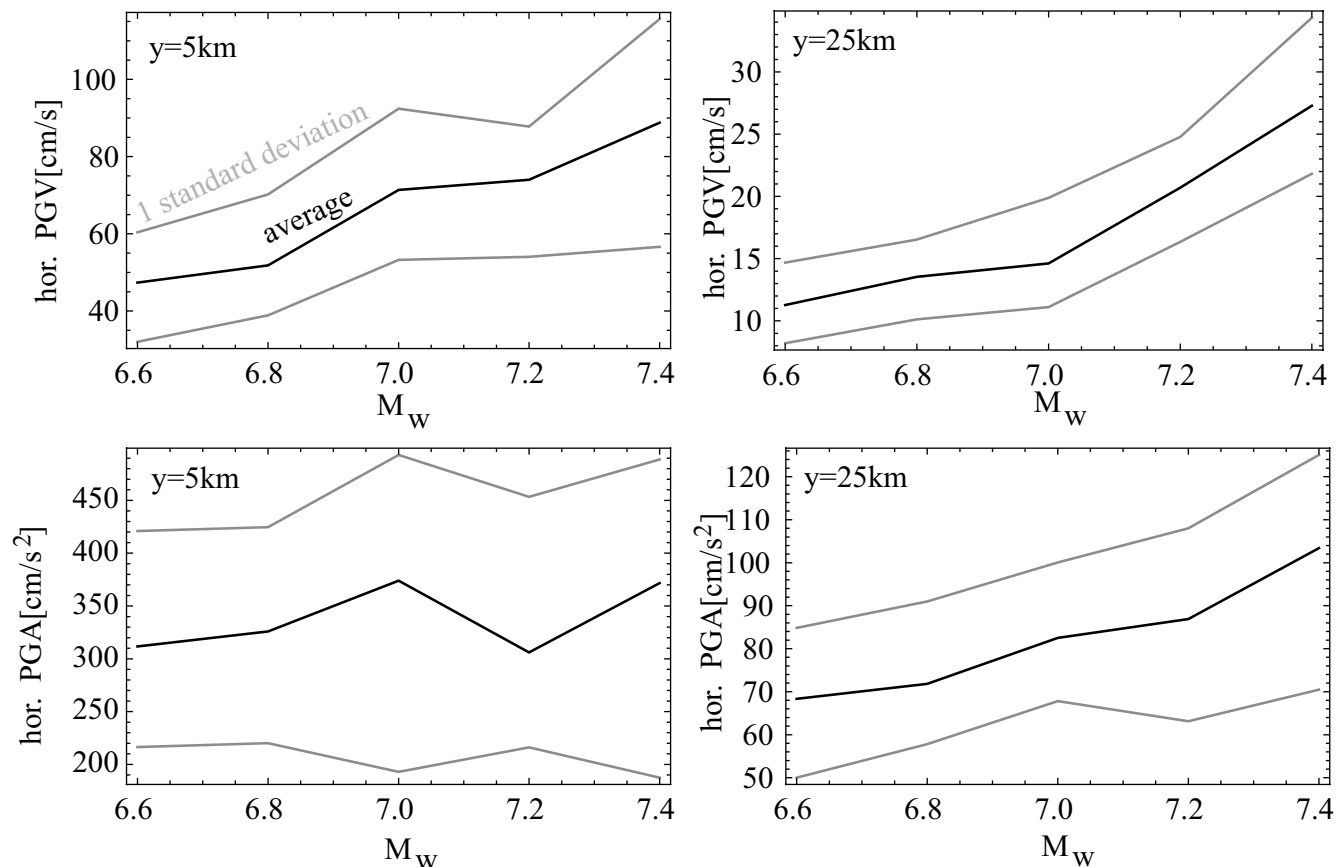


Figure 12. Average ± 1 standard deviation for 50 horizontal PGA and PGV values for each magnitude and for distances of $y = 5$ km and $y = 25$ km. The 50 values were randomly selected from ground motions computed for six different random kinematic source models for each magnitude. Distance dependent magnitude scaling for PGA is evident. That is, for stations close to the fault (for example, $y = 5$ km), PGA saturates with magnitude; farther from the fault (for example, $y = 25$ km) PGA increases with magnitude.

constant and close distance from the fault, the profile of PGA and PGV shows an initial increase in amplitude and then a decrease as one moves along strike from the epicenter. That is, close to the fault there is no monotonous increase of peak ground motion along the rupture plane as could be expected by directivity. For the homogeneous case—constant slip, rupture velocity, and rise time—the shape of the along strike profiles can be explained using the concept of the critical point. At the critical point, future isochrones get discontinuous, and a large change in the isochrone contribution occurs. This radiates a strong phase that produces the maximum amplitude for stations in the proximity of the critical point. Because the critical point stays at about the same position, geometrical attenuation reduces the radiation for stations farther along strike (but at constant y), leading to smaller PGV and PGA. Consequently, when plotting PGA and PGV as a function of distance from the epicenter along strike, they increase to a maximum and then decrease to lower values.

For a fixed distance perpendicular to the fault, we use the critical point to construct a predictor for the location of the maximum PGV and PGA along strike. This predictor is also useful for comparing different scenarios because geometries that resulted in smaller PGV always resulted in a

smaller predictor. We examined scenarios with different distances H between the hypocenter and the top of the fault. For smaller H we compute a smaller maximum PGV. The predictor also yields a smaller value. This suggests that the position of the hypocenter relative to the top boundary of the fault is an important factor in the prediction of peak values in ground motion and may explain the observations of Somerville (2003).

For heterogeneous rupture models in a layered medium, the shape of the PGV profile along strike has similar characteristics to that for the homogeneous model: (1) along strike profiles at a fixed distance to the fault show an increase of PGV and PGA to a maximum and decreasing values afterwards, and (2) the position of the maximum is farther along strike for larger distances (y) from the fault.

These characteristics directly affect empirical attenuation relations that mostly use a distance measure similar to the perpendicular distance to the fault (Abrahamson and Shedlock, 1997). Empirical relations show saturation of PGA and also PGV with increasing magnitude close to the fault (Abrahamson and Silva, 2008; Boore and Atkinson, 2008; Campbell and Bozorgnia, 2008; Chiou and Youngs, 2008). Given our results this can be explained in two ways. First, by

increasing the fault length of long ruptures, the maximum PGV and PGA are not increased significantly, but the likelihood of a station to be in the tail of the rupture that has low amplitudes increases. Consequently, peak ground motion smaller than the maximum peak ground motion along strike is more likely to be sampled. The maximum ground motion for a given distance from the fault does not decrease; it is just less likely to be sampled by increasing the length of the rupture. Second, even if there were full station coverage, the average PGV and PGA at a fixed y would likely saturate because more values smaller than the maximum are included in the averaging process for large magnitude events.

All of our computations were made for strike-slip faults in a homogeneous medium and a 1D layered medium. We expect similar conclusions in a medium that is weakly heterogeneous in 3D though we have not shown this. We have shown that magnitude saturation of PGA and PGV can be expected for sites located close to long strike-slip faults.

Data and Resources

No data were used in this article. Figure 1 was modified from Boore and Atkinson (2008). The kinematic models were computed using the code by Liu *et al.* (2006). The resulting seismograms were analyzed using Mathematica, version 6.0, by Wolfram Research, Inc.

Acknowledgments

We thank Raul Madariaga who clearly explained the significance of the critical point in the isochrones and its effect on ground motions, and we thank Paul Spudich for pointing out the need to include a fourth term in equation (1). We thank Yuehua Zeng for providing this term and explaining its consequences. Furthermore, we thank Michel Bouchon, Joe Fletcher, and Martin Vallée for helpful comments that greatly improved this manuscript. This work was supported by the Southern California Earthquake Center (SCEC). SCEC is funded by the National Science Foundation (NSF) Cooperative Agreement Number EAR-0106924 and U.S. Geological Survey (USGS) Cooperative Agreement Number 02HQAG0008. This is SCEC Contribution Number 1202 and the Institute for Crustal Studies (ICS) Contribution Number 0874.

References

- Abrahamson, N. A., and K. M. Shedlock (1997). Overview, *Seism. Res. Lett.* **68**, 9–23.
- Abrahamson, N., and W. Silva (2008). Summary of the Abrahamson & Silva NGA ground motion relations, *Earthq. Spectra* **24**, 67–97.
- Anderson, J. G. (2000). Expected shape of regressions for ground-motion parameters on rock, *Bull. Seismol. Soc. Am.* **90**, S43–S52.
- Andrews, D. J. (1976). Rupture velocity of plane strain shear cracks, *J. Geophys. Res.* **81**, 5679–5687.
- Archuleta, R. J. (1984). A faulting model for the 1979 Imperial Valley earthquake, *J. Geophys. Res.* **89**, 4559–4585.
- Bernard, P., and R. Madariaga (1984). A new asymptotic method for the modeling of near-field accelerograms, *Bull. Seismol. Soc. Am.* **74**, 539–557.
- Boore, D. M., and G. M. Atkinson (2008). Ground motion prediction equations for the average horizontal component of PGA, PGV, and 5%-damped PSA at spectral periods between 0.01 s and 10 s, *Earthq. Spectra* **24**, 99–138.
- Bouchon, M., and M. Vallée (2003). Observation of long supershear rupture during the magnitude 8.1 Kunlunshan earthquake, *Science* **301**, 824–826.
- Bouchon, M., M. P. Bouin, H. Karabulut, M. N. Toksöz, M. Dietrich, and A. Rosakis (2001). How fast is rupture during an earthquake? New insights from the 1999 Turkey earthquakes, *Geophys. Res. Lett.* **28**, 2723–2726.
- Burridge, R. (1973). Admissible speeds for plane-strain shear cracks with friction but lacking cohesion, *Geophys. J. R. Astron. Soc.* **35**, 439–455.
- Campbell, K. C., and Y. Bozorgnia (2008). Campbell-Bozorgnia NGA horizontal ground motion model for PGA, PGV, PGD, and 5% damped linear elastic response spectra, *Earthq. Spectra* **24**, 139–171.
- Chiou, B., and R. Youngs (2008). An NGA model for the average horizontal component of peak ground motion and response spectra, *Earthq. Spectra* **24**, 173–215.
- Cua, G. B. (2004). Creating the virtual seismologist: developments in ground motion characterization and seismic early warning, *Ph.D. Thesis*, California Institute of Technology, Pasadena, California, 408 p.
- Dunham, E. M., and R. J. Archuleta (2004). Evidence for a supershear transient during the 2002 Denali Fault earthquake, *Bull. Seismol. Soc. Am.* **94**, S256–S268.
- Kagawa, T., K. Irikura, and P. G. Somerville (2004). Difference in ground motion and fault rupture process between the surface and buried rupture earthquakes, *Earth Planets Space* **56**, 3–14.
- Lavallée, D., and R. Archuleta (2003). Stochastic modeling of slip spatial complexities for the 1979 imperial valley, California, earthquake, *Geophys. Res. Lett.* **30**, 1245, doi 10.1029/2002GL015839.
- Liu, P., R. J. Archuleta, and S. H. Hartzell (2006). Prediction of broadband ground-motion time histories: hybrid low/high-frequency method with correlated random source parameters, *Bull. Seismol. Soc. Am.* **96**, 2118–2130.
- Mai, P. M., and G. C. Beroza (2002). A spatial random field model to characterize complexity in earthquake slip, *J. Geophys. Res.* **107**, 2308.
- Rogers, A. M., and D. M. Perkins (1996). Monte Carlo simulation of peak-acceleration attenuation using a finite-fault uniform-patch model including isochrone and extremal characteristics, *Bull. Seismol. Soc. Am.* **86**, 79–92.
- Somerville, P. G. (2003). Magnitude scaling of the near fault rupture directivity pulse, *Phys. Earth Planet. Inter.* **137**, 201–212.
- Spudich, P., and B. S.-J. Chiou (2008). Directivity in NGA earthquake ground motions: analysis using isochrone theory, *Earthq. Spectra* **24**, 279–298.
- Spudich, P., and L. N. Frazer (1984). Use of ray theory to calculate high-frequency radiation from earthquake sources having spatially variable rupture velocity and stress drop, *Bull. Seismol. Soc. Am.* **74**, 2061–2082.
- Wells, D. L., and K. J. Coppersmith (1994). New empirical relationships among magnitude, rupture length, rupture width, rupture area, and surface displacement, *Bull. Seismol. Soc. Am.* **84**, 974–1002.
- Zeng, Y. (1991). Deterministic and stochastic modeling of the high frequency seismic wave generation and propagation in the lithosphere, *Ph.D. Thesis*, University of Southern California, Los Angeles, California.
- Zhu, L., and L. A. Rivera (2002). A note on the dynamic and static displacements from a point source in multilayered media, *Geophys. J. Int.* **148**, 619–627.

Department of Earth Science and Institute for Crustal Studies
University of California
Santa Barbara, California 93106
ralph@crustal.ucsb.edu